ILL: 105661240

OCLC Number: 1695800

Request Type: COPY

Staff Email: docdelivery@cdc.gov

Billing Notes: EFTS/IFM

Call Number: 22-(1986-)

Location:

Maxcost: 20.00IFM

Source: ILLiad

Affiliation:

DateReq: 6/11/2013

Date Rec: 6/11/2013

Borrower: HNC

☐ Yes ☐ No ☐ Conditional

LenderString: *GMU,TKN,TNT,SSK,EYU

Title: IEEE transactions on industry applications.

Uniform Title:

Author:

Edition:

Imprint: [New York, Institute of Electrical and Electronic Engineers]

Article: 'Li, Jingcheng; Jobes-C; Carr-J' Comparison of magnetic field distribution models for a magnetic proximity detection system

Copyright: CCG

Vol: 49 No.: 3 Pages: 1171-1176 Date: May-June 2013

Dissertation:

Verified: <TN:1064933> OCLC 0093-9994

Borrowing Notes: GL$D member/Please email articles to docdelivery@cdc.gov (maxCost: $20.00)

ShipTo: CDC Library
1600 Clifton Rd NE
Bldg 19 First Floor MS-C04
Atlanta GA 30329-4018

E-delivery Addr:

Ship Via: Library Mail

ShipVia: **Library Mail**

Return To:

Jack Tarver Library
Mercer University
1300 Edgewood Avenue
Macon, GA 31207

Ship To:

CDC Library
1600 Clifton Rd NE
Bldg 19 First Floor MS-C04
Atlanta GA 30329-4018

NeedBy: 7/11/2013

Borrower: HNC

ILL: 105661240 Lender: GMU

Req Date: 6/11/2013 OCLC #: 1695800

Patron: ILL Gran , Marsha

Author:

Title: IEEE transactions on industry applications.

Article: 'Li, Jingcheng; Jobes-C; Carr-J' Comparison of magnetic field distribution models for a magnetic

Vol.: 49 No.: 3

Date: May-June 201 Pages: 1171-1176

Verified: <TN:1064933> OCLC 0093-9994

Maxcost: 20.00IFM Due Date:

Lending Notes:

Bor Notes: GL$D member/Please email articles to docdelivery@cdc.gov (maxCost: $20.00)

Comparison of Magnetic Field Distribution Models for a Magnetic Proximity Detection System

Jingcheng Li, Christopher C. Jobes, and Jacob L. Carr

Abstract—**Magnetic proximity detection technology is rapidly advancing as a promising method of protecting underground mine workers from striking and pinning hazards associated with mobile mining machines. A magnetic proximity detection system requires a magnetic distribution model to estimate the proximity of the sensor to the generators. This paper presents a comparative analysis of magnetic flux density distribution models in three different field distribution design patterns. The accuracy of these models is determined with a laboratory magnetic proximity detection system. These field distribution design patterns are spherical, ellipsoidal, and sphere-cosine, respectively. The analyses show that the sphere-cosine model is the most accurate model for the proximity system followed by the ellipsoidal and spherical models.**

Index Terms—**Collision avoidance, electromagnetic modeling, error analysis, ferrite device, magnetic fields, magnetic flux density, magnetic sensors, mining equipment, optimization.**

I. Introduction

A proximity detection system must determine the proximity of workers near a piece of mobile machinery and automatically act to prevent accidents. Low accuracy in such a safety system could result in a false alarm, or worse, a failure to alarm. Therefore, the accuracy of proximity detection systems, to a large extent, determines their safety value. These systems require an accurate magnetic flux density distribution model to precisely determine the proximity of a magnetic sensor to the system's magnetic generators. A magnetic flux density model provides a function that relates the magnetic flux density of a generator to the distance from that generator. Several possible model design patterns result in varying proximity detection system accuracies. Researchers at the National Institute for Occupational Safety and Health (NIOSH) have recently investigated the effect of using differing magnetic field distribution design patterns on the accuracy of a laboratory-based magnetic proximity detection system. Three different model design patterns or shapes were used in this investigation: the spherical model, the ellipsoidal model, and the sphere-cosine or NIOSH model.

Manuscript received July 1, 2011; accepted May 8, 2012. Date of publication February 1, 2013; date of current version May 15, 2013. Paper 2011-MIC-323, presented at the 2011 IEEE Industry Applications Society Annual Meeting, Orlando, FL, USA, October 9–13, and approved for publication in the IEEE TRANSACTIONS ON INDUSTRY APPLICATIONS by the Mining Industry Committee of the IEEE Industry Applications Society.

The authors are with the National Institute for Occupational Safety and Health, Office of Mine Safety and Health Research (OMSHR), Pittsburgh, PA 15236 USA (e-mail: Jingcheng .Li@cdc.hhs.gov; gtx2@cdc.gov; Christopher.jobes@cdc.hhs.gov; JacobCarr@cdc.hhs.gov).

Color versions of one or more of the figures in this paper are available online at http://ieeexplore.ieee.org.

Digital Object Identifier 10.1109/TIA.2013.2244546

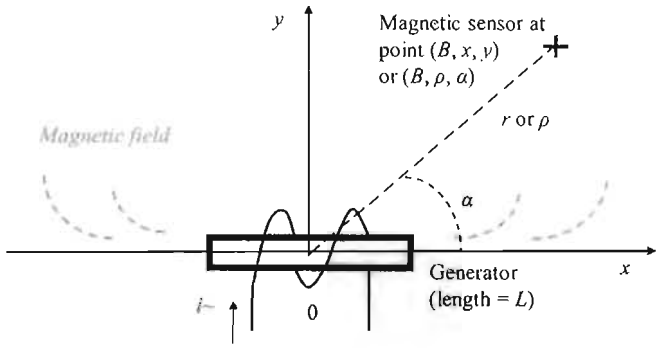

Fig. 1. Proximity detection system components: ferrite-cored generator and magnetic flux density sensor.

A. Background

Data from the Mine Safety and Health Administration show that, from 1999 to 2006, there were, on average, 254 accidents per year during routine mining and maintenance activities involving remote-control continuous mining machines (CMMs) in the United States. Since 1984, there have been 37 fatalities, in which a miner was crushed by a remote-control CMM. To reduce the accident and fatality rates involving CMMs and other types of equipment, some mining companies have begun to use magnetic proximity detection systems to protect workers. When workers enter an area where they could be struck by moving parts of the machine, these systems issue visual or auditory warnings and/or stop machine movement. It is not uncommon to find a worker within 1 or 2 m from a CMM in a mine entry. In such a situation, only a system with a degree of accuracy on the order of tens of centimeters will be able to provide effective protection for the worker.

A magnetic proximity detection system uses one or more magnetic generators to create a magnetic field around a machine. A magnetic sensor worn by a worker detects the magnetic field and estimates the proximity of the sensor to the generator based on a measured magnetic flux density. Fig. 1 shows the basic components of the systems in a 2-D overhead view, where r is the distance from the generator to the sensor in a direction determined by the angle α, and B is the magnetic flux density reading at the sensor. A magnetic flux density model is used to determine this distance based on the magnetic flux density reading. The accuracy of the calculated distance is governed by the magnetic flux density model used.

All points around a magnetic field generator that have the same magnetic flux density reading form what is known as a shell. The shape of a shell is determined by the magnetic flux density of the generated field and the distance from the magnetic field generator.

B. Magnetic Flux Density Models

A number of shell-based field distribution patterns can be used to model a magnetic field around a generator. A spherical shape is often used to approximate the field far away (far-field) from a generator. An ellipsoidal shape is frequently used in websites, presentations, and brochures by magnetic proximity detection system manufacturers to illustrate the magnetic field geometry near a generator. The sphere-cosine shape (see the Appendix) has been recently developed by researchers at NIOSH to approximate the field near to or far from a generator [1]. To evaluate these 3-D models for ferrite-cored generators, researchers at the NIOSH Office of Mine Safety and Health Research performed these evaluations in their 2-D forms for simplicity and clarity. Because of the axially symmetric nature of the magnetic field, the 2-D evaluation results should apply generally to the 3-D models. The circular-shelled model (circular model) is the 2-D form for the sphere-shelled model, the ellipse-shelled model (elliptical model) is the 2-D form for the ellipsoid-shelled model, and the circle-cosine-shelled model (NIOSH model) is the 2-D form for the sphere-cosine-shelled model.

Equation (1) is a general expression of the circular model for a single generator, with the symbols and the coordinate system shown in Fig. 1. Equation (2) defines the elliptical model. Equation (3) defines the NIOSH model. In these equations, L is the length of the generator; c and d in (1c); c_a, d_a, c_b, and d_b in (2b) and (2c); and c_a, d_a, c_b, and d_b in (3d) and (3e) are constants for a given steady magnetic field that can be determined through flux density measurements [1]. With these constants determined, the corresponding magnetic shell function can be generated for any arbitrary B from each of these models. Equations (1a) and (1b) are the shell function for the circular model in Cartesian coordinates and (1c) in polar coordinates. Equation (2a) is the shell function for the elliptical model. Equations (3a) and (3b) are the shell function for the NIOSH model in Cartesian coordinates and (3c) in polar coordinates.

The radius for the circular model, i.e., r, can be obtained for a measured B from the polar circular shell function (1c), and the (x, y) values of the points on the shell can then be found from the Cartesian shell functions (1a) and (1b). The values of the semimajor axis a and semiminor axis b for the elliptical model can be obtained for a measured B from (2b) and (2c). All the points on the ellipse-shell will satisfy the shell function (2a). Shell parameters a and b for the NIOSH model can be obtained for a measured B from (3d) and (3e). The magnitude of the distance, i.e., ρ, to a point on the shell can be calculated from the polar shell function (3c) by varying the angle α, and the (x, y) values of the points on the shell can then be calculated from Cartesian shell functions (3a) and (3b) in the same way. All shells in the circular and elliptical models look similar regardless of the shell sizes. However, any two shells may have very different shapes for the NIOSH model, as illustrated in Fig. 2. As shown in (3d) and (3e), the B reading determines not only the size of a shell but also its shape

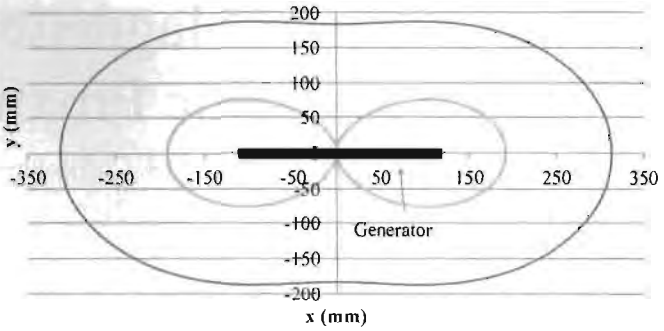

Fig. 2. Two examples of shells from the NIOSH model.

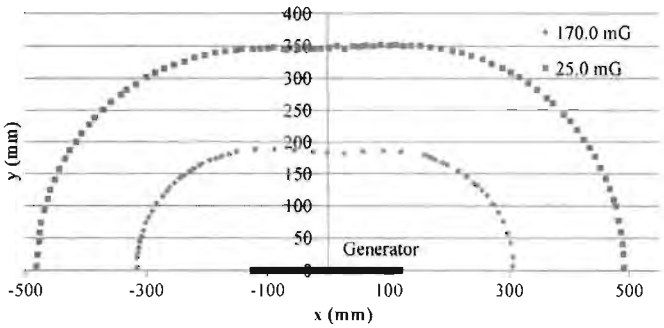

Fig. 3. Actual measured points for two shells.

$$\left.\begin{matrix}\text{shell}_c(x,y|B)\\ \text{shell}_c(r,\alpha|B)\end{matrix}\right\} = \begin{cases} x = r\cos(\alpha) & \text{(1a)}\\ y = r\sin(\alpha) & \text{(1b)}\\ \quad 0 \le \alpha \le 2\pi & \\ r = cB^{-d} & \text{(1c)}\end{cases} \tag{1}$$

$$\text{Shell}_c(x,y|B) = \begin{cases} (x/a)^2 + (y/b)^2 = 1 & \text{(2a)}\\ a = c_a B^{-d_a} & \text{(2b)}\\ b = c_b B^{-d_b} & \text{(2c)}\end{cases} \tag{2}$$

$$\left.\begin{matrix}\text{Shell}_N(x,y|B)\\ \text{Shell}_N(\rho,\alpha|B)\end{matrix}\right\} = \begin{cases} x = \rho\cos(\alpha) & \text{(3a)}\\ y = \rho\sin(\alpha) & \text{(3b)}\\ \rho = \alpha\cos(2\alpha) + b & \text{(3c)}\\ \quad 0 \le \alpha \le 2\pi & \\ a = c_a B^{-d_a} & \text{(3d)}\\ b = c_b B^{-d_b} & \text{(3e)}\\ \quad a + b \ge L/2. & \end{cases} \tag{3}$$

II. Model Comparison

The plots shown in Fig. 3 are two of many sets of actual magnetic flux density measurements from a proximity detection system. Each of the sets contains measurements for an individual shell, i.e., constant B. These two sets of measurements will be used to build the shells for the circular, elliptical, and NIOSH models for an evaluation of these models in this section. The generator used in the system has a 25 × 25 × 304.8 mm Mn–Zn ceramic core of type MN60-2573-970-07. An IDR-200 Gauss meter is used to measure magnetic flux density B in units of milligauss (mG).

The optimal shell functions for the circular, elliptical, and NIOSH models were constructed using procedures similar to those introduced in [1] from each of the individual data sets. The shell data shown in Fig. 3 were processed and yielded (4)

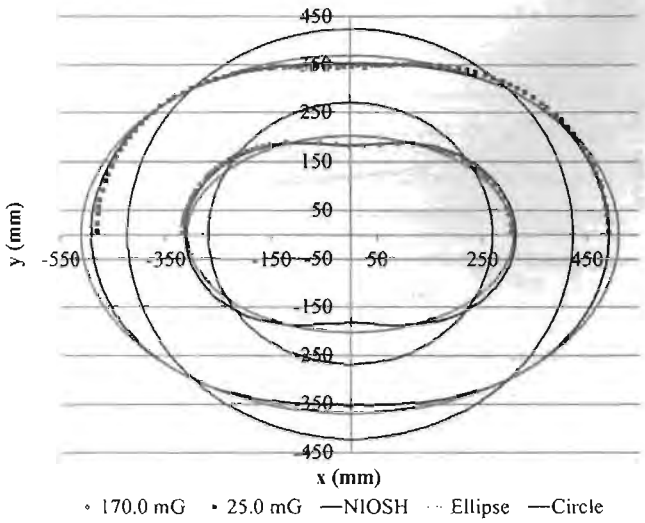

Fig. 4. Plots of the shell models generated from actual measurements.

for $B = 170.0$ mG and (5) for $B = 25.0$ mG, where (4a), (4c), (5a), and, (5c) are in polar coordinates and (4b) and (5b) in Cartesian coordinates for convenience. The plots of these functions along with the actual measurements are shown in Fig. 4. Clearly, the NIOSH model fits the actual measurements best

$$\begin{cases} \text{Circle} : r = 269.31 & (4a) \\ \text{Ellipse} : (x/309.04)^2 + (y/201.71)^2 = 1 & (4b) \\ \text{NIOSH} : \rho = 65.03\cos(2\alpha) + 248.21 & (4c) \\ \quad 0 \le \alpha \le 2\pi \end{cases} \quad (4)$$

$$\begin{cases} \text{Circle} : r = 422.74 & (5a) \\ \text{Ellipse} : (x/510.21)^2 + (y/368.97)^2 = 1 & (5b) \\ \text{NIOSH} : \rho = 69.04\cos(2\alpha) + 422.71 & (5c) \\ \quad 0 < \alpha < 2\pi. \end{cases} \quad (5)$$

The standard deviations of the modeling errors, and both absolute and relative maximum modeling errors, are shown in Fig. 5(a) and (b) for these shells. As shown in the figures, the maximum relative modeling error for the elliptical model is 4.6 times as great as the NIOSH model for $B = 170$ mG and 2.5 times for $B = 25.0$ mG; the maximum relative error for the circular model is 20.7 times as great as the NIOSH model for $B = 170$ mG and 8.9 times for $B = 25.0$ mG.

As shown in Fig. 5(a) and (b), the difference of the relative maximum modeling errors (2.29% and 2.51%) for the NIOSH model for $B = 170.0$ mG and $B = 25.0$ mG is very small. This indicates that the major contributions to those errors are the resolution and accuracy limitations of the proximity system and the inevitable ambient magnetic noise, implying that these errors are local, and should be independent of location and distance to the generator. In contrast, the difference of the relative maximum modeling errors (10.46% and 6.31%) for the elliptical model for $B = 170.0$ mG and $B = 25.0$ mG is far greater than those for the NIOSH model. This indicates that, in addition to the resolution and accuracy limitation of the system and the ambient noise, a model pattern design error is introduced by the elliptical model, meaning that the elliptical shape never fits an actual magnetic shell, although it might approach it at greater distances. The same analysis applies to the circular model, but it is even less favorable. The relative errors for both the elliptical and circular models are clearly dependent

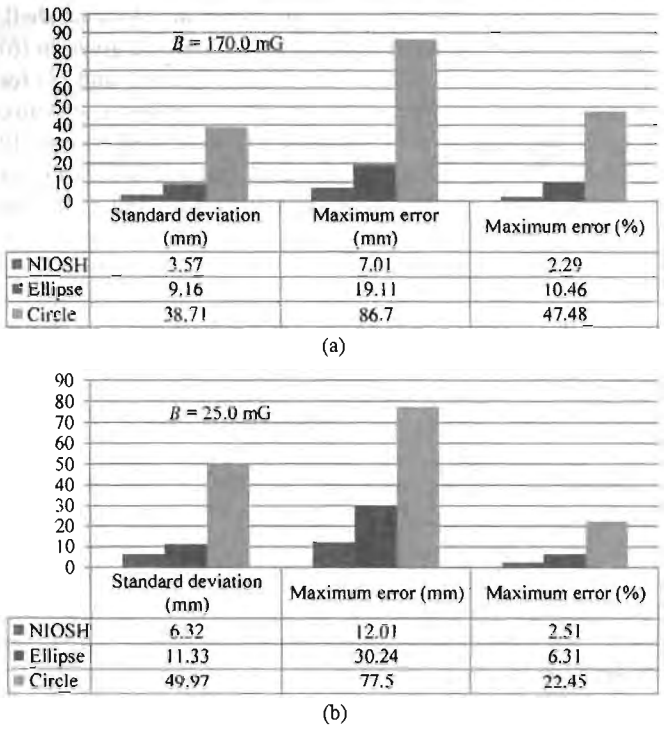

Fig. 5. Error statistics for shell models of different shapes with (a) $B = 170.0$ mG and (b) $B = 25.0$ mG.

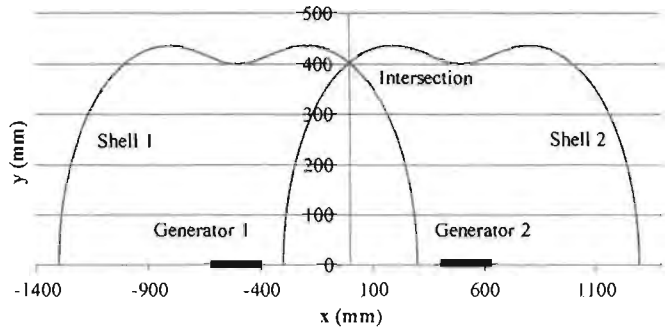

Fig. 6. Intersection of two magnetic shells.

on location and distance, implying the global and nonuniform distribution nature of these errors.

III. Positioning Accuracy Comparison for Different Models

As demonstrated in [3], the position of a sensor can be determined as the intersection of two or more magnetic shells in a multigenerator system. To determine the impact of these models on positioning accuracy, an experiment was conducted, in which two generators were used to determine position. The intersection of two magnetic shells from the generators was used as the calculated position for the sensor in a plane, as illustrated in Fig. 6. (The intersection of two half-shells was used in the actual implementation.) In this experiment, two similar generators with a size of 25.4 × 25.4 × 304.8 mm were laid 1 m apart on a wooden platform and were alternately running.

Prior to the positioning test, 18 sets of measurement data similar to those shown in Fig. 3 with B readings from 5.0 to 297.0 mG were collected from the generators. Each data set

contained the measurements of 25 points for an individual shell. From these data, the models were constructed and given in (6) for the circular model, (7) for the elliptical model, and (8) for the NIOSH model, in their local generator coordinate systems. Procedures similar to those given in [1] were used to equally and optimally determine the models' constants to establish a fair comparison base [refer to c and d in (1c), c_a and d_a in (2b) and (3d), and c_b and d_c in (2c) and (3e)] for these models, as shown in Fig. 7(a)–(e).

To make a statistical evaluation of the calculated positions possible, 40 actual points were selected in the global coordinate system, as shown in Fig. 8. The measurements at these points were denoted by $(x_i, y_{i,}, B_{i1}, B_{i2})$, $i = 1, 2, 3, \ldots, 40$, where x_i and y_i were coordinates at the ith point, and B_{i1} and B_{i2} were magnetic flux density readings from generators 1 and 2, respectively, at the ith point. B_{i1} and B_{i2} were used to generate the two corresponding shells. The intersection of these two shells was taken as the calculated position of the sensor. Fig. 9 shows the plots of these calculated positions from the three different models against the actual points. As shown in Fig. 9, the calculated positions with the NIOSH model are closest to the actual points; those using the elliptical model come in second; those using the circular model show the largest differences from the actual points. Fig. 10 shows the error statistics of the calculated positions for each of the different models. The relative maximum positioning error is 3.26 times for the elliptical model and 10.83 times for the circular model over that of the NIOSH model, as shown in Fig. 11.

As shown in Figs. 9 and 10, the calculated positions with the NIOSH model show not only the smallest statistical error in every category but also uniform accuracy over the entire space. This indicates that the major contributions to the errors are the local measurements and magnetic noise. In contrast, the calculated positions with the elliptical and circular models show not only greater errors than with the NIOSH model in every category but also a nonuniform distribution of the errors in the area. The apparent dependence on location and distance of the positioning accuracy indicates that the model pattern design errors are inherent and that they propagate through the system positioning calculations. Although the model pattern errors from two generators might cancel each other at some calculated points resulting in a slight positioning error, this is not a reliable technique to systematically compensate for the model pattern design errors. Thus

$$\left.\begin{matrix}\text{shell}_c(x, y|B)\\ \text{shell}_c(r, \alpha|B)\end{matrix}\right\} = \begin{cases} x = r\cos(\alpha) & (6a)\\ y = r\sin(\alpha) & (6b)\\ \quad 0 \le \alpha < 2\pi & \\ r = 1852.1B^{-0.323} & (6c)\end{cases} \quad (6)$$

$$\text{Shell}_c(x, y|B) = \begin{cases} (x/a)^2 + (y/b)^2 = 1 & (7a)\\ a = 2047.8B^{-0.305} & (7b)\\ b = 1783.5B^{-0.348} & (7c)\end{cases} \quad (7)$$

$$\left.\begin{matrix}\text{Shell}_N(x, y|B)\\ \text{Shell}_N(\rho, \alpha|B)\end{matrix}\right\} = \begin{cases} x = \rho\cos(\alpha) & (8a)\\ y = \rho\sin(\alpha) & (8b)\\ \rho = a\cos(2\alpha) + b & (8c)\\ \quad 0 \le \alpha < 2\pi & \\ a = 165.04B^{-0.186} & (8d)\\ b = 1846.7B^{-0.324} & (8e)\\ \quad a + b \ge 152.4 \text{ mm} & \end{cases} \quad (8)$$

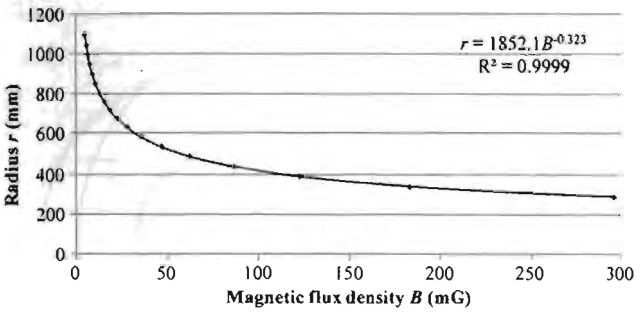

(a)

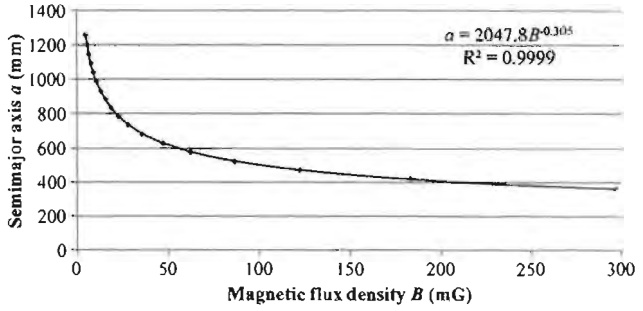

(b)

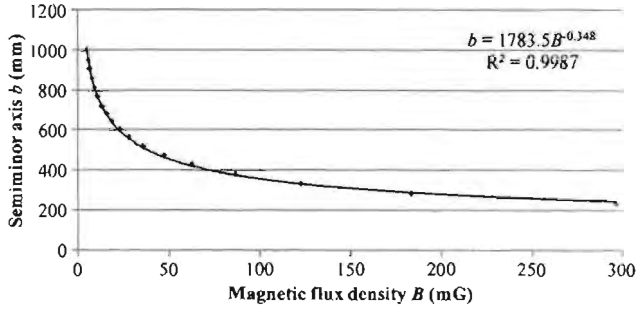

(c)

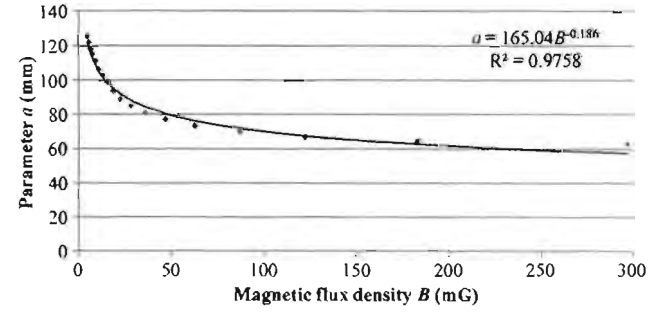

(d)

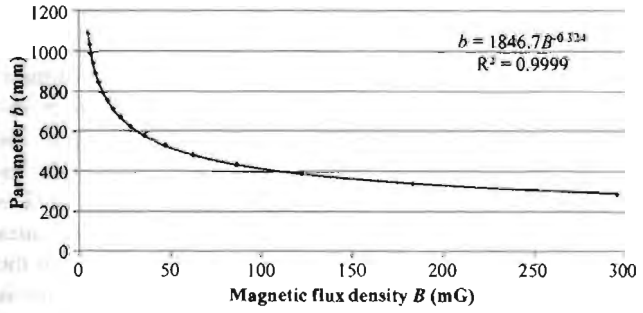

(e)

Fig. 7. (a) Optimal radius for the circular model. (b) Optimal semimajor axis a for the elliptical model. (c) Optimal semiminor axis b for the elliptical model. (d) Optimal field parameter a for the NIOSH model. (e) Optimal field parameter b for the NIOSH model.

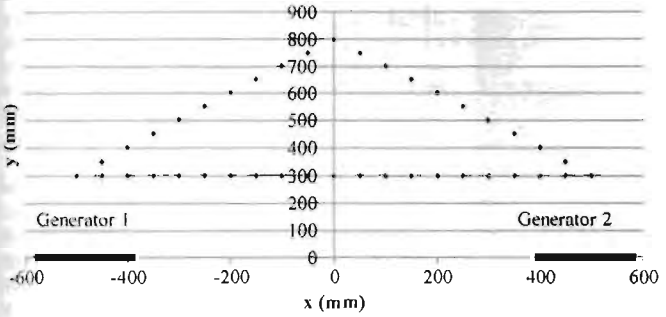

Fig. 8. Actual points on the global coordinate system.

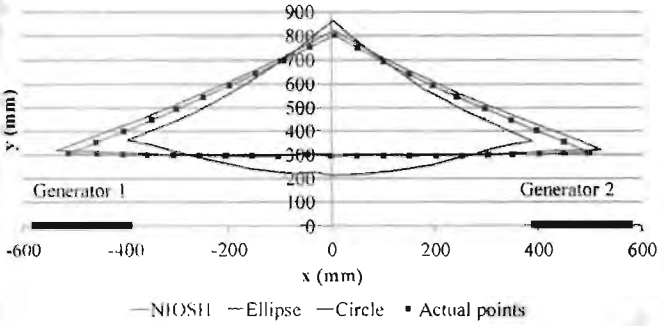

Fig. 9. Calculated positions by using different models against the actual points.

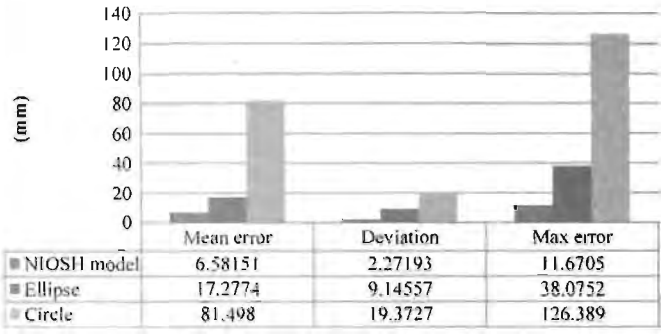

	Mean error	Deviation	Max error
NIOSH model	6.58151	2.27193	11.6705
Ellipse	17.2774	9.14557	38.0752
Circle	81.498	19.3727	126.389

Fig. 10. Positioning errors resulting from different models.

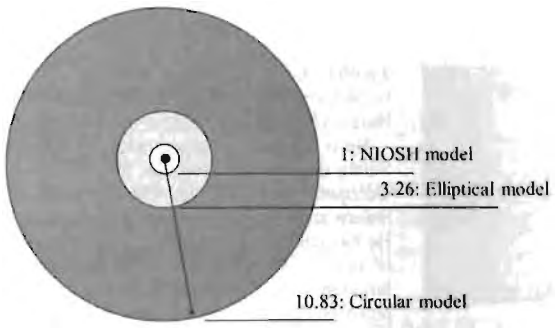

Fig. 11. Relative maximum positioning calculation errors from different models.

IV. Discussion

The comparative analysis in this presentation suggests that the NIOSH model accurately characterizes the intrinsic magnetic flux density distribution of ferrite-cored generators used in mediums with relatively uniform permeability. Many additional error-inducing factors, such as various metal parts of a machine,

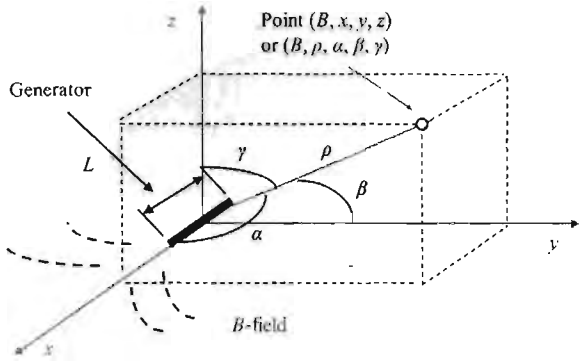

Fig. 12. Three-dimensional coordinates for the magnetic generator.

will be introduced in an actual proximity detection system in working environments, which may distort the system's magnetic flux density distribution pattern. These factors can be considered as independent variables to study for a system in working environments. The magnetic model that accurately captures the fundamental magnetic flux density distribution should not only result in good system accuracy but also be advantageous in isolating and evaluating those additional error-inducing factors. Such a model should produce slight error to impede the investigation of the error contributions from those factors.

V. Conclusion

Three magnetic flux density distribution modeling patterns in their 2-D forms (circle, ellipse, and circle-cosine or NIOSH) have been used to model the magnetic fields generated by a magnetic proximity detection system. Among them, the NIOSH model exhibits the best match to the actual magnetic flux distribution shapes over the extended space around a generator. The elliptical and circular models both show noticeable modeling errors due to their mismatches with the actual magnetic field shape. The modeling errors are nonuniformly distributed, and the maximum errors with these two models can be many times greater than those from the NIOSH model. Because of the propagation of these modeling errors, proportional positioning errors are also seen. The positioning errors also exhibit in a nonuniformly distributed manner and are dependent on distance and location for the elliptical and circular models. These errors highlight not only the high positioning accuracy but also the uniformly distributed accuracy of the NIOSH model.

Appendix

The original NIOSH sphere-cosine magnetic flux density model for the ferrite-cored generator of magnetic proximity detection systems [1] is shown in (9), with the symbols and the coordinate system shown in Fig. 12, where (9a) and (9b) are the shell functions in Cartesian and direction cosine systems, respectively, and a and b are shell parameters, which can be determined from (9c) and (9d), respectively, with a given magnetic flux reading B. Parameters c_a and d_a in (9c) and c_b and d_b in (9d) are constants for a given steady magnetic field.

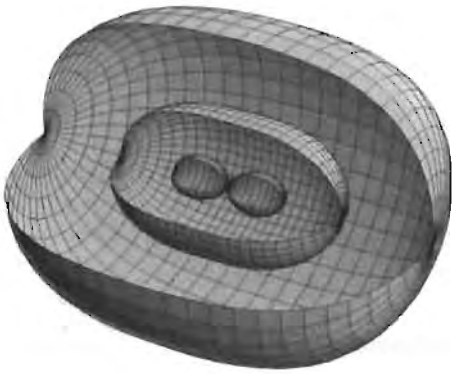

Fig. 13. Plots of three magnetic shells.

Fig. 13 shows what the magnetic shells look like. These shell functions are determined from actual measurements [1]. Thus

$$\text{Shell}(x,y,z|B) \text{ or } \text{Shell}(\rho,\alpha,\beta,\gamma|B)$$

$$== \begin{cases} (x^2+y^2+z^2)^{1/2} = a\left(\frac{x^2-y^2-z^2}{x^2+y^2+z^2}\right)+b & \text{(9a)} \\ \rho = a(\cos^2\alpha - \cos^2\beta - \cos^2\gamma)+b & \text{(9b)} \\ \quad 0 \le \alpha,\beta,\gamma < \pi & \\ a = c_a B^{-d_a} & \text{(9c)} \\ b = C_b B^{-d_b} & \text{(9d)} \\ \quad a+b \ge L/2. & \end{cases} \quad (9)$$

ACKNOWLEDGMENT

The authors would like to thank J. DuCarme and A. Jobes for their help in data collection and processing, R. Unger for his support of this paper, and Dr. J. A. Waynert for his suggestions in presentation of the data. The findings and conclusions in the paper are those of authors and do not necessarily represent the views of the NIOSH.

REFERENCES

[1] J. Li, J. Carr, and C. Jobes, "A shell-based magnetic field model for magnetic detection systems," *Safety Sci.*, vol. 50, no. 3, pp. 463–471, Mar. 2012.
[2] J. Li, J. Carr, and J. Bartels, "Modeling of the magnetic field around a ferrite-cored generator in a proximity detection system," in *Proc. 14th Conf. Electromagn. Field Comput.*, Chicago, IL, USA, May 9–12, 2010, p. 1.
[3] J. Carr, C. Jobes, and J. Li, "Development of a method to determine operator location using electromagnetic proximity detection," in *Proc. Int. Workshop Robot. Sensors Environ.*, Phoenix, AZ, USA, Oct. 15/16, 2010, pp. 1–6.
[4] W. Schiffbauer, "Active proximity warning system for surface and underground mining applications," *Mining Eng.*, vol. 54, no. 12, pp. 40–48, 2002.
[5] J. Bartels, S. Gallagher, and D. Ambrose, "Continuous mining: A pilot study of the role of visual attention locations and work position in underground coal mines," *Prof. Safety*, vol. 54, no. 8, pp. 28–35, Aug. 2009.
[6] J. Bartels, D. Ambrose, and S. Gallagher, "Analyzing factors influencing struck-by accidents of a moving mining machine by using motion capture and DHM simulations," in *Proc. Digit. Human Model. Des. Eng. Conf. Exhib.*, Pittsburgh, PA, USA, Jun. 17–19, 2008.

Jingcheng Li received the B.S. degree in electrical engineering from the China University of Mining and Technology, China, in 1982 and the M.S. and Ph.D. degrees in mining engineering specializing in electrical engineering applications from The Pennsylvania State University, University Park, PA, USA, in 1992 and 1996, respectively.

He is a Senior Service Fellow with the National Institute for Occupational Safety and Health, Office of Mine Safety and Health Research, Pittsburgh, PA, USA. His primary research interests include underground communication and tracking and proximity detection. In particular, he is currently focusing on investigation of the medium-frequency propagation characteristics in underground mines and the modeling of magnetic field distribution and precise locating architecture of magnetic proximity detection systems. Previously, he was a Senior Software Engineer with Analog Devices, Inc. (ADI). Prior to ADI, he was an Instructor with the Department of Electrical and Automation Engineering, China University of Mining and Technology.

Dr. Li received the first prize paper award and the prize paper award in 1995 and 2000, respectively, both shared with Dr. J. Kohler from the IEEE.

Christopher C. Jobes received two Bachelor's degrees from Geneva College, Beaver Falls, PA, USA, and the Master's and Doctorate degrees from West Virginia University, Morgantown, WV, USA, where he developed a variable-speed robot controller and a remotely controllable residential circuit breaker.

He is a Mechanical Engineer performing research with the National Institute for Occupational Safety and Health (NIOSH), Office of Mine Safety and Health Research (OMSHR), Pittsburgh, PA, USA. After receiving the Bachelor's degrees, he worked as a Software Programmer/Consultant for a year. From 1987 to 1997, he was with the U.S. Bureau of Mines, working in control and navigation of a computer-assisted mining machine, earning his professional engineering certification from Pennsylvania in 1989. Since then, he has been with NIOSH, working in the fields of software safety, mining equipment safety, and jolting and jarring abatement in mining machinery while also acting as an Adjunct Professor of mechanical engineering at Geneva College. He is currently conducting leading-edge research in electromagnetic proximity detection of mining personnel and its attendant visual warning system to improve underground equipment safety.

Jacob L. Carr received the B.S. and M.S. degrees in mining engineering from the University of Nevada, Reno, NV, USA.

He is a Mining Engineer with the Office of Mine Safety and Health Research, National Institute for Occupational Safety and Health, Office of Mine Safety and Health Research, Pittsburgh, PA, USA. He has conducted research on the computer control of surface mining equipment, underground mine illumination, and mining machine safety. He is currently leading a research project aimed at developing and testing two novel safety technologies: intelligent proximity detection for continuous mining machines and other mobile equipment and intelligent lockout/tagout for belt conveyors and other stationary equipment.